Applied Catalysis B: Environmental 150–151 (2014) 93–100

Contents lists available at ScienceDirect

Applied Catalysis B: Environmental

journal homepage: www.elsevier.com/locate/apcatb

Modeling intrinsic kinetics in immobilized photocatalytic microreactors

Aura Visan [a], Damon Rafieian [a], Wojciech Ogieglo [b], Rob G.H. Lammertink [a,*]

[a] Soft Matter, Fluidics and Interfaces, MESA+Institute for Nanotechnology, University of Twente, P.O. Box 217, 7500 AE Enschede, The Netherlands
[b] Membrane Science and Technology, MESA+Institute for Nanotechnology, University of Twente, P.O. Box 217, 7500 AE Enschede, The Netherlands

ARTICLE INFO

Article history:
Received 5 October 2013
Received in revised form
30 November 2013
Accepted 2 December 2013
Available online 12 December 2013

Keywords:
Photocatalysis
Microreactor
Intrinsic kinetics
Thiele modulus
Internal effectiveness factor

ABSTRACT

The article presents a simple model for immobilized photocatalytic microreactors following a first order reaction rate with either light independency or light dependency described by photon absorption carrier generation semiconductor physics. Experimental data obtained for various residence times, catalyst thicknesses and photon flux densities proved that the model is capable of describing the reactor performance. The extracted reaction rate constant reveals the intrinsic kinetics as both external and internal mass transport are accounted for. The effect of light is also considered by defining a criterion for neglecting light intensity based on film thickness and absorption coefficient. For the first time k values on the order of magnitude of 10^1 s^{-1} are reported. In the end, performance parameters are also derived for the light dependent model for which the internal effectiveness factor reveals both mass transfer and light limitations.

1. Introduction

Heterogeneous photocatalysis is a promising technology for environmental remediation. However, commercial products are focused mostly on self-cleaning surfaces and air filtering. Important applications such as removing refractory compounds from wastewater are scarce. In 2007 van Gerven et al. [1] mentioned only 6 examples: Zentox Corporation, Matrix Photocatalytic Inc., Clearwater Industries, Photox Bradford Ltd., Lynntech Inc. and Purifics Environmental Technologies Inc. The invoked reasons are small conversion capacities and inefficient light use, addressing especially the inconsistencies in the definitions of various performance parameters. A progress in optimization requires that individual research efforts can be combined which is possible only if an honest comparison between them can be achieved.

One parameter used frequently when evaluating the conversion capacity of a reactor is the apparent reaction rate constant. Its derivation implies identifying the reaction rate with the conversion $-dc/dt = r$. The kinetic model is usually Langmuir–Hinshelwood $r = kKc/(1 + Kc)$ or a first order reaction $r = kc$ from which the reaction rate constant is obtained [2–10]. The agreement with respect to these basic relations is widespread, as several reviews mention it [11,12].

Heterogeneous reactions involve the diffusion of species to the active catalyst sites. Mass transport becomes important and if omitted can alter the true values of the reaction kinetics. Intrinsic kinetic parameters are of paramount importance. They are required for catalyst screening and necessary when simple engineering tools such as the apparent reaction constant are used for comparing different reactor configurations. The real value for the reaction rate constant allows the evaluation of the mass transfer contribution on the conversion which is a main factor dictating the performance of a reactor. Evidently, comparison complicates further when the gradients in photon absorption become important and kinetics cannot be volume averaged anymore. When both immobilized and dispersed systems are considered, the difference in light dispersion can be bridged only by light dependent intrinsic kinetics.

The standard approach for kinetic investigation is to place the system in the reaction rate limiting regime, so the apparent reaction rate can reach the intrinsic value. The classical method uses a differential reactor which consists of a reaction chamber and a mixing tank, where the reaction volume is much smaller than the total volume. The small conversion per pass allows the simplification of the mass balance to a batch reactor equation. The intrinsic kinetics are determined for flowrate – independent conversions [13–24]. Accepting the reliability of this method to eliminate external mass transport, the question about internal mass transfer remains, which will be present even for thin catalyst layers or for an inevitable degree of aggregation in slurry systems. Ballari et al. [25–27] went on to defining guidelines for canceling mass transfer limitations in

* Corresponding author. Tel.: +31 534894798; fax: +31 534892882.
E-mail address: r.g.h.lammertink@utwente.nl (R.G.H. Lammertink).

0926-3373/$ – see front matter © 2013 Elsevier B.V. All rights reserved.
http://dx.doi.org/10.1016/j.apcatb.2013.12.003

slurry reactors based on flow rate, catalyst loading and irradiation rates.

Even when concentration gradients are eliminated, the inhomogeneity regarding light distribution has to be carefully considered, especially for slurry systems. Motegh et al. [28] gave guidelines for operating in optically differential mode. Starting from the premise of perfect mixing, a criterion was defined for keeping the gradients in photon absorption rate small enough as to allow the volume-averaging of the reaction rate.

A more thorough method is to model light distribution, fluid dynamics and mass transfer and fit the kinetics to the experimental data. Due to the complexity of large-scale photocatalytic reactors, a lot of assumptions come into play.

The first challenge in a large-scale system is the non-uniform incident flux. To obtain the radiation field distribution, light emission models have to be correlated to the radiation transfer equation (RTE) in order to obtain the local volumetric rate of energy absorption (LVREA) which can be afterwards coupled to the reaction rate. In case of dispersed systems, the radiation transfer equation becomes more complex due to in and out-scattering effects that also depend on the aggregation extent of the particles [29–33].

The next step is to consider the complex hydrodynamics. The most rigorous approach is to perform a CFD simulation which solves the continuity and Navier–Stokes equations and also requires turbulence models. Again, dispersed systems demand the most elaborate models. An Eulerian multi-fluid approach is necessary to connect the fluid velocity field to the solid particle distribution. However, real flow computations are quite challenging. This is why, when possible, approximations are used. In case of small deviations from laminar flow, the axial dispersed model can be considered. For this, the Péclet number (Pe) can be experimentally determined from RTD measurements [34,35]. At the other end of the complexity spectrum, perfect laminar or turbulent flows are the most convenient options.

Once the velocity field is characterized, mass transport can be investigated. The most accepted approximation for slurry reactors is a one phase system with high Pe numbers. Hence, the governing equation represented advection and homogeneous reaction only [36–38].

For immobilized systems it is easier to couple the reaction rate to mass transfer, given the clear definition for the interface. The most realistic transport models for the flow channel take into account both advection and diffusion [39–43]. All these studies neglect the internal mass transport inside the catalyst film. Hence, the reaction rate is set as the boundary condition for the catalyst–fluid interface. A more manageable method is to represent mass transport through the stagnant film model. The mass transfer coefficient can be determined experimentally with the benzoic acid dissolution method [44,45] or can be computed via empirical correlations from Reynolds and Schmidt numbers [46–49].

Microreactors are a special case. The modeling of such systems is straightforward due to their laminar flow and constant photon flux density throughout the entire surface of the reactor. Moreover, for immobilized catalyst, interface scattering due to roughness is neglected. Bulk scattering is not relevant due to absorption. Hence, the RTE simplifies to a Lambert–Beer law.

Very few papers seem to exploit the potential for accurate modeling of microreactors. Most of the articles employ the PFR equation [50–53]. Meng et al. [53] report values for reaction rate constants without providing an equation. It is assumed the same PFR equation is used due to its widespread use. Gorges et al. [50] validate the intrinsic character of k by proving their system is placed in the reaction limiting regime. Lindstrom et al. [54] adopts the same approach of employing Damköhler number to assess mass transfer restrictions. However, for the apparent reaction rate constant they use the highest value in the literature, without computing the one for their system.

Charles et al. [55] used the axially dispersed plug flow model to set up the mass balance in the microreactor. Mass transfer in the radial direction was represented by the stagnant film. Both the axial dispersion and mass transfer coefficients were computed from empirical relations. The kinetic model was initially Langmuir–Hinshelwood, but later on simplified to a first order-like equation. The kinetic coefficients were fitted to the model via iteration.

Nielsen et al. [56] derived a reaction rate expression based on semiconductor physics. The governing equation they set up for the catalyst layer comprised of diffusion and reaction. The gas concentration in the flow channel was considered constant by keeping the conversion under 10%. They also managed to define a continuity equation for the localized excess hole concentration.

The current article draws attention on the simplicity of accurate modeling in the case of microreactors and proposes them as a pertinent choice when attempting to extract kinetic parameters. A complete model for immobilized photocatalytic microreactors is set up for the first time and solved for both light independency and light dependency first order kinetics. Experimental data obtained for various residence times, catalyst thicknesses and photon flux densities proves the model is capable of describing the reactor performance. Furthermore, a criterion is defined based on the absorption coefficient and catalyst thickness to mark the transition toward the regime where the incorporation of photon flux density is required. Performance parameters are also derived for the light dependent model for which the internal effectiveness factor reveals both mass transfer and light limitations.

The potential of the models is not confined to microreactor engineering. Scale-up is straightforward compared to slurry reactors as only channel height and catalyst thickness should be designed for a specific flowrate.

2. Materials and methods

2.1. Microreactor fabrication

The silicon chips cut from 4 in. wafers were cleaned with 65% nitric acid (Merck) for 15 min and rinsed with water and acetone. Following the cleaning, the substrates were covered entirely with a commercial TiO_2 suspension (VP Disp. W 2730 X, Evonik) and spin coated at 3000 rpm angular velocity and 524 rpm/s acceleration. The spin coating time was kept at 1 min. The resulted layer was sintered for 2 h at 500 °C in air. The heating and cooling rates were kept at 2 °C/min.

The standard thickness obtained with the unprocessed dispersion of 30 wt.% solid content was around 1200 nm. Thinner layers were prepared by decreasing the viscosity of the dispersion. 310 nm and 640 nm were obtained by diluting the dispersion with distilled water to 15 and respectively 24% solid content. Thicker films were prepared by multiple coatings with sintering in between. The alteration of photocatalytic activity by repeated sintering was ruled out when the same degradation was observed for layers with one and two sintering cycles. As a general rule, the thickness of the catalyst layer was multiplied by the number of coatings.

Catalytic films of 310, 640, 1200, 2050, 3000 and 4000 nm were used for degradation experiments.

The microreactor was assembled by attaching the TiO_2 coated substrate to a PDMS slab containing the microchannel replicated from a microstructured mold. The PDMS was prepared by blending the polymer base (RTV-615 A, Permacol) with the curing agent

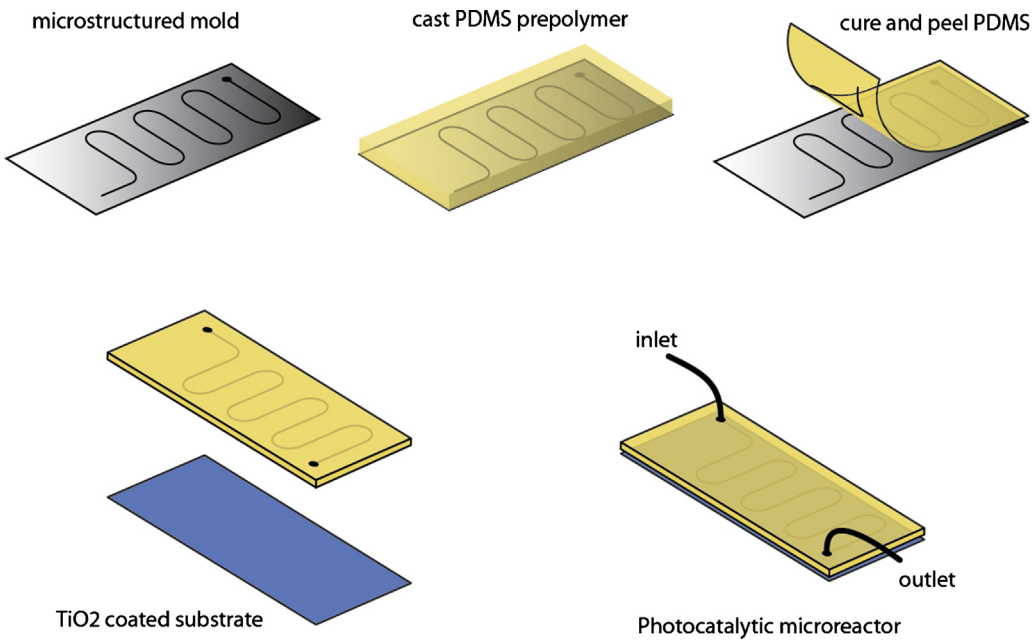

Fig. 1. Schematic of the micro reactor fabrication steps. PDMS is cast on a microstructures mold and released after curing. The PDMS slab is subsequently sealed to a TiO_2 coated substrate.

(RTV-615 B, Permacol) in 10:1 ratio as indicated by the manufacturer. The mixture was poured on top of a patterned wafer and degassed in a vacuum desiccator. After partial curing for 45 min at 60 °C, while still preserving its adhesive properties, the PDMS slabs were cut out from the mold, punctured for the inlet and outlet connections, attached to the substrate containing the catalyst layer and cured for another 45 min. To ensure a leakfree assembly, additional PDMS was poured and cured for 3 h at 70 °C. The inlet and outlet connections were made by introducing needles into the previously punctured holes. The preparation steps are illustrated in Fig. 1.

The microstructured mold was made by standard photolithography using negative photoresist (SU-8). SU-8 was spun on silicon wafer at 500 rpm for 10 s and continued to 100 rpm for 30 s. Then the sample was prebaked at 50, 65, 95 °C for 10, 10, 45 min respectively. This is followed by UV exposure for 33 s and post baking at 50, 65, 80 °C for 5, 10, 20 min respectively. Finally the sample was spray developed by RER 600. The resulted SU-8 height was measured with optical profiler. The channel is rectangular and follows a meandering path. The basic dimensions are: 50 μm height, 500 μm width and 5.96 cm length, with a total volume of 1.49 μL.

2.2. Catalyst layer characterization

High resolution SEM showed a highly homogeneous surface with a narrow particle size distribution around 20 nm. The cross-section (Fig. 2) shows also a uniform porosity throughout the layer.

M2000-X variable angle spectroscopic ellipsometer by J.A. Woollam was used for fast and non-invasive thickness measurements. The accuracy of the method was validated by comparing one of the results with the value obtained from SEM. Porosity and roughness could also be extracted by ellipsometry measurements. Porosity was determined by the Bruggeman Effective Medium Approximation, EMA [57] by mixing properties of dense TiO_2 and void in a self consistent manner. Bruggeman type of EMA was used because it is well valid when the volume fractions of both components are comparable. Roughness was also estimated using EMA, this time adding a layer on top of the samples with assumed 50% of material and 50% of void and fitting its thickness. Values

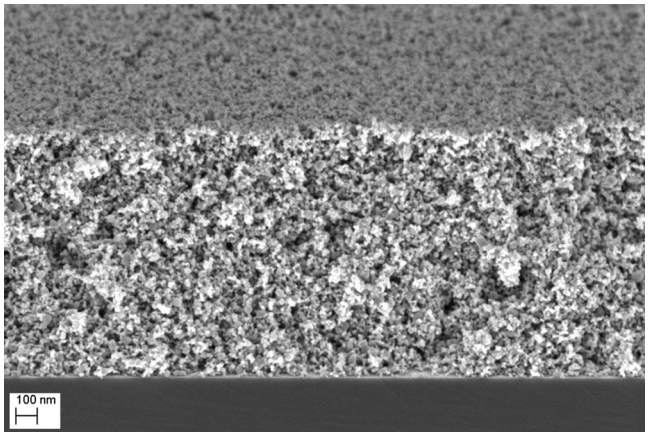

Fig. 2. SEM cross-section of a porous TiO_2 film.

of 45% and 10 nm, respectively, were consistent for thicknesses ranging between 300 and 4000 nm. The morphology of layers is reproducible due to the same spin coating parameters used during preparation.

Ellipsometry could also be used for evaluating optical constants. Due to the homogeneity of the film, scattering was almost absent. Consequently, the model fitted very well and the accuracy of the measurement was high. For the extinction coefficient determination, we modeled the dielectric dispersion of the material by parametrization with B-Splines which is basically a polynomial spline function [58]. It works well when normal parametrization of the dielectric function requires too many dielectric oscillators. We also forced the dispersion to be Kramers–Kronig consistent, namely physically viable.

The extinction coefficient can be easily converted to absorption coefficient (Fig. 3) using the formula: $\alpha = 4\pi\beta/\lambda$ where β is the extinction coefficient, α is the absorption coefficient (1/nm) and λ is the wavelength (nm). The method was validated by comparing the results with the absorption coefficient computed from transmission measurements of TiO_2 films of varying thickness (Fig. 4). The transmission measurements were performed by connecting a

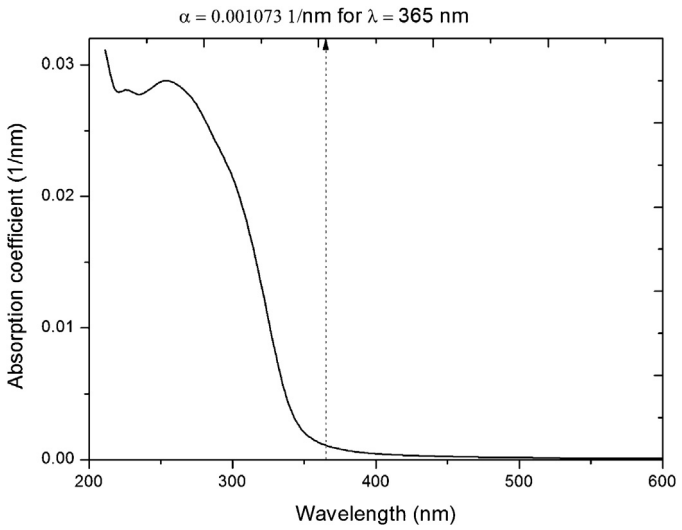

Fig. 3. Spectral absorption coefficient of a TiO_2 layer.

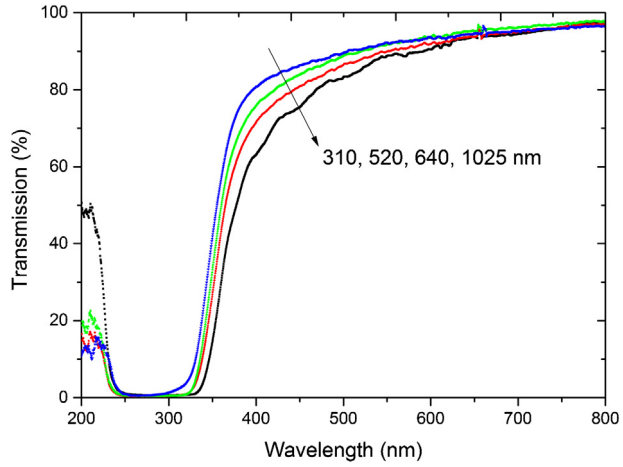

Fig. 4. Transmission spectra for multiple catalyst thicknesses.

FHS-UV In-Line Filter Holder (Ocean Optics) to the UV-VIS spectrometer (USB2000+Miniature Fiber Optic Spectrometer by Ocean Optics) where the substrate coated with the catalyst film was fixed. Quartz glass was used as a substrate due to its transparency in the far UV range. Cleaned quartz glass was used to reference the transmission. The absorption coefficient was extracted only for a single wavelength as a mere validation tool from the slope of the straight line fitting $-ln(T/100)$ against thickness based on the Lambert–Beer law: $T = I/I_0 \cdot 100 = e^{-\alpha \Delta x}$.

2.3. Microreactor operation

An aqueous solution of 10 mg/L cortisone 21-acetate (CA) (Sigma–Aldrich) was injected into the microreactor with flowrates of 5, 10, 20, 30, 40 and 50 μL/min using a syringe pump.

The CA concentration was determined by light absorbance measurements using USB2000+Miniature Fiber Optic Spectrometer (Ocean Optics). The monitored wavelength was 244.48 nm, corresponding to the maximum absorption peak of CA. The calibration was carried out for different concentrations of CA solutions (from 5 to 20 mg/L).

When adsorption reached steady state and the concentration recorded by the UV-VIS spectrometer showed the inlet value, the UV lamp (UV-Point Source HP-120, Dr. Gröbel UV-Electronik GmbH) was turned on. The photocatalytic degradation of CA was continuously monitored by passing the outlet stream through a flowcell connected to the spectrometer. For the first batch of experiments, the irradiance was set at 180 W/m^2. For the second part, the light intensity was varied between 55 and 270 W/m^2 by changing the distance between the light guide and the microreactor. Due to the sharp emission peak, there was no necessity for integrating the irradiance over the whole TiO_2 absorbing wavelength range. The total incoming photon flux density was approximated to the value corresponding to 365 nm wavelength which was measured using an optical power meter (Newport 1916-R).

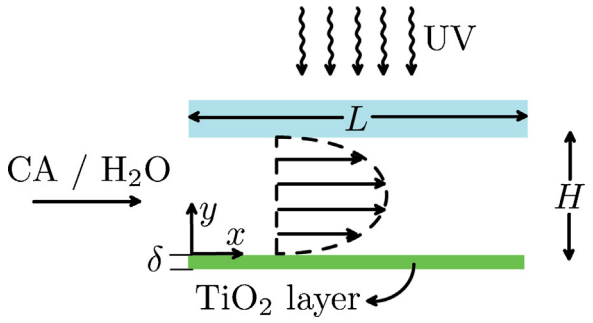

Fig. 5. Schematic representation of the 2D model, indicating channel length L, channel height H, and catalyst thickness δ.

O_2 was continuously replenished through the permeable PDMS layer. The O_2 permeability of the PDMS layer was tested by monitoring the O_2 concentration after passing O_2 depleted water through the reactor. The O_2 inline detector recorded a steady state concentration very close to the maximum solubility of O_2 in water at atmospheric pressure.

3. Model

3.1. Light independent model

Fig. 5 illustrates the schematics of the model. The reactor was divided into 2 domains: the flow channel and the catalyst film.

The governing equation in the catalyst layer includes diffusion and reaction only. The reaction rate is assumed to be first order with respect to the cortisone acetate, zero order with respect to oxygen due its provision through the permeable PDMS layer and zero order with respect to irradiance. Hence, the mass balance for the catalyst layer reduces to:

$$D_{eff} \frac{\partial^2 c}{\partial y^2} - kc = 0 \quad (1)$$

where $D_{eff} = D \cdot \epsilon/\tau$ is the effective diffusion coefficient, D is the molecular diffusion coefficient for cortisone acetate in water, ϵ is the porosity, τ is the tortuosity and k is the first order reaction rate constant.

The bottom boundary for the catalyst layer has the flux equal to zero:

$$y = -\delta : D_{eff} \frac{\partial c}{\partial y} = 0 \quad (2)$$

The boundary condition at the interface between the channel and the catalyst is represented by flux and concentration continuity:

$$y = 0 : c = c_L, D_{eff} \cdot \frac{\partial c}{\partial y} = D \frac{\partial c_L}{\partial y} \quad (3)$$

The diffusion reaction equation together with the boundaries mentioned above have the following analytical solution:

$$c(y) = c_L \cdot \frac{cosh(\phi \cdot (1 + y/\delta))}{cosh(\phi)} \quad (4)$$

where Thiele modulus is $\phi = \sqrt{k/D_{eff}} \cdot \delta$.

Hence, the domain of the catalyst layer can be collapsed into a single flux boundary condition for the flow channel:

$$N_{y=0} = D_{eff} \cdot \frac{\partial c}{\partial y} = \frac{D_{eff} \cdot \phi \cdot c_L}{\delta} \cdot tanh(\phi) \quad (5)$$

The transport of the model compound in the flow channel is governed by advection and diffusion.

$$u(y) \cdot \frac{\partial c_L}{\partial x} = D \cdot \frac{\partial^2 c_L}{\partial y^2} \quad (6)$$

where $u(y) = u_{avg} \cdot (-6y^2/H^2 + 6y/H)$ represents a parabolic velocity profile.

The governing equation for the flow channel was non-dimensionalized to a square 1×1 domain (Eq. (7)) together with the boundary conditions (Eqs. (8) and (9)) and numerically solved in Matlab.

$$u_{avg} \cdot (-6y'^2 + 6y') \cdot \frac{1}{L} \cdot \frac{H^2}{D} \cdot \frac{\partial c'}{\partial x'} = \frac{\partial^2 c'}{\partial y'^2} \quad (7)$$

where $x' = x/L$, $y' = y/H$, $c' = c_L/c_0$.

$$N_{y'=0} = \frac{D_{eff} \cdot \phi \cdot c' \cdot H}{\delta} \cdot tanh(\phi) \quad (8)$$

for the boundary to the catalytic coating.

$$N_{y'=1} = D \frac{\partial c'}{\partial y'} = 0 \quad (9)$$

for the upper wall.

3.2. Light dependent model

To account for light dependent conversion, the photon flux density was incorporated in the reaction rate described by photon absorption carrier generation first order kinetics. The expression was taken form Nielsen et al. [56], derived based on semiconductor physics. The governing equation for the catalyst layer becomes:

$$D_{eff} \frac{\partial^2 c}{\partial y^2} - kc \left(\frac{\alpha \Phi_0}{Bp_0 n_0 \hbar\omega} \right)^{\gamma} exp(-\gamma\alpha y) = 0 \quad (10)$$

where $Bp_0 n_0 \cong 3.3 \times 10^{-23}\ m^{-3}\ s^{-1}$ is the equilibrium electron–hole recombination rate [56], Φ_0 is the incoming photon flux density, $\hbar\omega$ is the photon energy, γ is the transfer coefficient for the electron transfer process and α is the absorption coefficient.

Given that the boundary conditions remain the same, the new analytical solution for the concentration profile in the catalyst layer becomes:

$$c(y) = c_L \cdot \frac{I1(2\phi\sqrt{e^{\gamma\alpha\delta}}/\gamma\alpha\delta) \cdot K0(2\phi\sqrt{e^{-\gamma\alpha y}}/\gamma\alpha\delta) + K1(2\phi\sqrt{e^{\gamma\alpha\delta}}/\gamma\alpha\delta) \cdot I0(2\phi\sqrt{e^{-\gamma\alpha y}}/\gamma\alpha\delta)}{I0(2\phi/\gamma\alpha\delta) \cdot K1(2\phi\sqrt{e^{\gamma\alpha\delta}}/\gamma\alpha\delta) + K0(2\phi/\gamma\alpha\delta) \cdot I1(2\phi\sqrt{e^{\gamma\alpha\delta}}/\gamma\alpha\delta)} \quad (11)$$

where $\phi^2 = k_i \cdot \delta^2/D_{eff} \cdot (\alpha\Phi_0/Bp_0 n_0 \hbar\omega)^{\gamma}$ and $I_n(x)$ and $K_n(x)$ are modified Bessel functions of the first and second kind.

This translates in the following boundary condition for the flow channel, giving the flux toward the catalyst layer which is again non-dimensionalized and implemented in Matlab:

$$N_{y'=0} = \frac{D_{eff} \cdot \phi \cdot H \cdot c'}{\delta} \cdot \frac{I1(2\phi\sqrt{e^{\gamma\alpha\delta}}/\gamma\alpha\delta) \cdot K1(2\phi/\gamma\alpha\delta) - K1(2\phi\sqrt{e^{\gamma\alpha\delta}}/\gamma\alpha\delta) \cdot I1(2\phi/\gamma\alpha\delta)}{I0(2\phi/\gamma\alpha\delta) \cdot K1(2\phi\sqrt{e^{\gamma\alpha\delta}}/\gamma\alpha\delta) + K0(2\phi/\gamma\alpha\delta) \cdot I1(2\phi\sqrt{e^{\gamma\alpha\delta}}/\gamma\alpha\delta)} \quad (12)$$

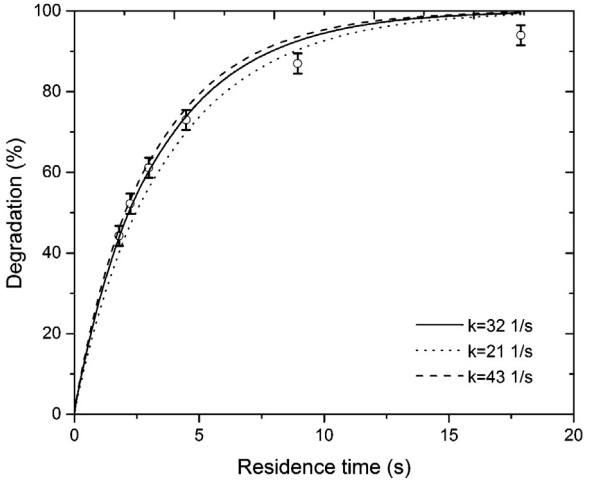

Fig. 6. Degradation of cortisone acetate (CA) vs. residence time for 2050 nm catalyst layer.

Note that the governing equation is the same for both the light dependent and light independent model, and that the two models only differ in the boundary condition describing the flux into the catalyst layer.

The geometry of the channel was simplified to a rectangle preserving the height, H, of 50 μm and the length, L, of 5.96 cm. The mesh was refined such that mesh independent results were obtained.

4. Results and discussion

4.1. Light independent model (LIM)

The assumption for a first order reaction rate was first justified by evaluating the effect of different residence times ranging between 1.8 and 18 s. The degradation vs. residence time curve, shown in Fig. 6, corresponds to 2050 nm catalyst thickness in order to capture the complete spectrum for the residence time range used during the experiments.

$k = 31\ s^{-1}$ was extracted by fitting the model for the lowest residence time where experimental data is more reliable. The reaction rate constant values determined for various catalyst thicknesses ranged between 21 and $43\ s^{-1}$. Their corresponding degradation curves were also plotted in Fig. 6. The standard deviation for the degradation is around ±2.5%. It was assessed based on the systematic deviation of the base line during the absorption measurements.

The consistency of k is set out in Fig. 7 where degradation is plotted against catalyst thickness ranging between 300 nm and 4000 nm for multiple residence times. An optimum catalyst thickness can already be deduced given the fact that an increase in thickness beyond 2000 nm affects the degradation only slightly.

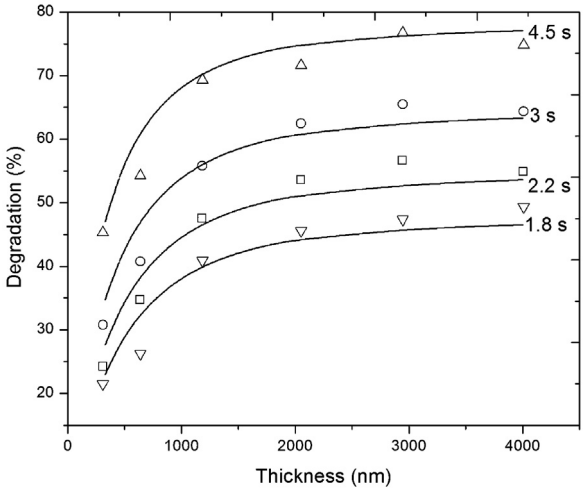

Fig. 7. Degradation vs. thickness for multiple residence times. Symbols depict experimental results and lines correspond to the light independent model with $k = 32\,s^{-1}$.

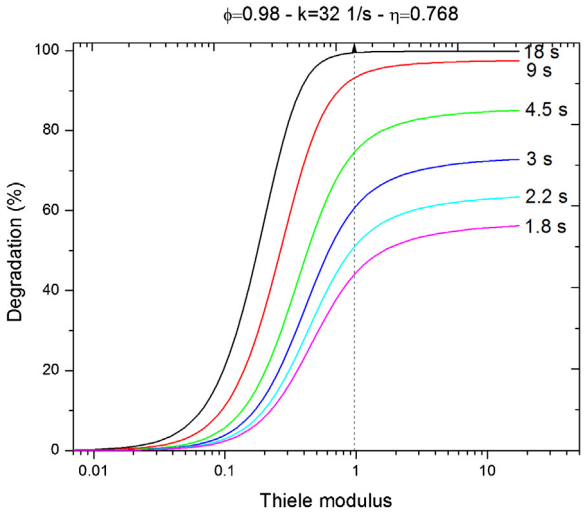

Fig. 8. Degradation by 2050 nm catalyst layer vs. Thiele modulus for multiple residence times.

The intrinsic k values are several orders of magnitude higher than the apparent first order reaction rate constants reported in the literature. For example, for methylene blue (MB), a common model compound, values between 10^{-5} and $10^{-2}\,s^{-1}$ are usually assigned [3,10,52,53,59–69]. The values increase for smaller reactor scales, reaching approximately $0.3\,s^{-1}$ for the present study. Following the same experimental routine and simulation procedure, given the molecular diffusion coefficient for MB in water, $D = 5.7 \times 10^{-10}\,m^2/s$, a value of $k = 40\,s^{-1}$ was fitted. The difference of two orders of magnitude between the real and apparent reaction rate constant draws attention on the importance of accurate modeling. The intrinsic value for the reaction rate constant allows catalyst comparison, as well as the evaluation of mass transfer for different reactor configurations.

The use for the extracted reaction rate constant can also be extended to different catalyst densities or dispersed systems by expressing it per unit surface area. The conversion from k per unit volume $[s^{-1}]$ to k'' per units surface area [m/s] has the known formula: $k'' = k/S_a\rho_c(1-\epsilon)$, where $S_a = 9 \times 10^4\,m^2/kg$ is the specific surface area, $\rho_c = 3895\,kg/m^3$ is the anatase density and $\epsilon = 0.45$ is the porosity. Consequently, MB has $k'' = 2.07 \times 10^{-7}$ m/s corresponding to $k = 40\,s^{-1}$, while CA has $k'' = 1.66 \times 10^{-7}$ m/s corresponding to $k = 32\,s^{-1}$.

Not to forget, the use of light independent kinetics is valid when the reaction rate can be volume averaged with respect to the field of local volumetric rate of photon absorption. The case of immobilized systems will be discussed later by comparing the light independent with the light dependent model.

For a quantitative optimization, the diffusion/reaction limiting regimes were investigated by evaluating the effect of k on degradation, in terms of Thiele modulus. For a first order reaction occurring in a planar porous catalyst, the Thiele modulus can be computed using the following formula: $\phi = \sqrt{k/D_{eff}} \cdot \delta$. The overall degradation given by a 2050 nm catalyst film was plotted in Fig. 8 against Thiele modulus for k ranging between 10^{-3} and $10^4\,s^{-1}$.

As k and, consequently, Thiele modulus start to increase, the intrinsic chemical reaction rate starts to compete with the given diffusion rate. For the experimentally determined kinetics, $k = 32\,s^{-1}$, $D_{eff} = 1.4 \times 10^{-10}\,m^2/s$ and $\delta = 2050$ nm, Thiele modulus is 0.98.

We will later analyze the effectiveness of the catalyst according to this model, combined with the light dependent model.

4.2. Light dependent model (LDM)

An important part in designing a photocatalytic reactor is related to light intensity distribution as effective use of light has a big impact on the economics of the process.

Whenever kinetics are modeled with respect to light intensity, I, the reaction rate is considered to follow a power law: $r = bI^{\gamma}$. Based on semiconductor physics, the physical meaning of γ would be the transfer coefficient of the electron transfer process. There is a general misunderstanding about γ, which is usually confused with the apparent γ extracted by fitting the conversion against the irradiance using a power law.

The real decrease in γ given by the higher enhancement in the recombination rate in connection with the excess hole production rate was found to happen at light intensities higher than $250\,W/m^2$ [70]. Moreover, values lower than 1 would translate in decreased efficiency regarding the use of light, rendering this operating range with less practical value.

The model was evaluated for the effect of different incoming photon flux densities. Fig. 9 shows the degradation by the 2050 nm catalyst film plotted against irradiance for values ranging between 55 and $270\,W/m^2$.

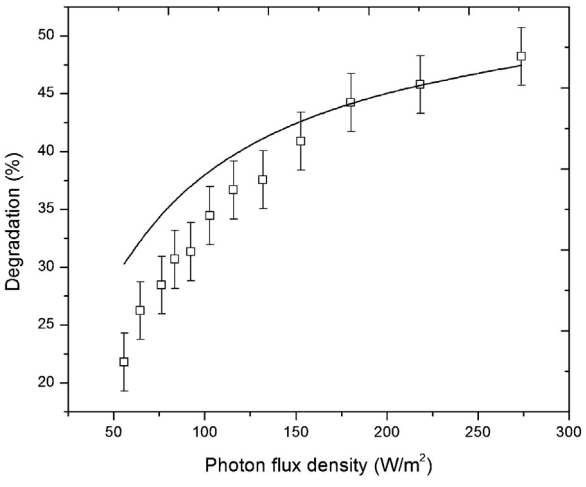

Fig. 9. Degradation by 2050 nm catalyst layer vs. photon flux density. $k_i = 6.46 \times 10^{-48}\,s^{-1}$, $\alpha = 1.073 \times 10^6\,1/m$, $\gamma = 1$.

For the light dependent reaction rate, $r = k_i(\alpha\Phi_0/Bp_0n_0\hbar\omega)^{\gamma}exp(-\gamma\alpha y)\cdot c$, the constant k_i was extracted by fitting the model to the experimental data for the higher light intensities. In this range, degradation is almost independent on the light intensity. The small order of magnitude $k_i \cong 10^{-48}\ s^{-1}$ comes from the high value of the prefactor $(\alpha\Phi_0/Bp_0n_0\hbar\omega)^{\gamma} \cong 10^{49}$.

The challenge with the incorporation of light into the kinetic model does not come only from the increased difficulty in mathematical manipulation. The most important disadvantage is the high number of unknowns that come into play when attempting to understand the photon absorption carrier generation mechanism. Simple engineering tools are very important for reactor design and optimization. A simplistic model could pave the way toward a consensus regarding photocatalytic reactor design and optimization and speed up the industrial implementation. Hence, a thorough comparison between the two models was performed in order to identify the regime where the simplistic model is an admissible approximation.

4.3. Criteria for neglecting light intensity

Previously, k was averaged for multiple catalyst thicknesses. However, when light is modeled, k is no longer constant throughout the thickness and follows an exponential decay: $k(y) = k_i(\alpha\Phi_0/Bp_0n_0\hbar\omega)^{\gamma}exp(-\gamma\alpha y)$. We can define a characteristic decay length: $\delta = 1/\gamma\cdot\alpha = 932.3$ nm where the normalized $k(y)$, $k'(y) = exp(-\gamma\alpha y)$ decreases to $1/e$ of its initial value. This light decay length (LDL) is very useful in order to point out the transition toward the regime where light incorporation is recommended.

The significance of LDL can be visualized by plotting the normalized concentration profiles for both models shown in Fig. 10. To have a common starting point k_{LIM} was equalized to $k_{y=0} = k_i\cdot(\alpha\Phi_0/Bp_0n_0\hbar\omega)^{\gamma} = 69.485\ s^{-1}$. For thicknesses higher than LDL, the concentration profiles of the two models become significantly distinct.

4.4. Updated performance parameters

A conclusive discussion has to include performance parameter investigation, as the efficient use of catalyst is crucial to the design procedure [71]. Given the first order reaction in the planar porous catalyst for the LIM, the internal effectiveness factor has the well known expression: $\eta = \tanh(\phi)/\phi$, where $\phi = \sqrt{k/D_{eff}}\cdot\delta$. In the case of LDM, the expressions were derived based on definitions. The internal effectiveness factor represents the ratio between the actual reaction rate and the rate in the absence of concentration gradients. However, an easier way to find this is to use the flux at the surface of the catalyst which equals to the total reaction occurring inside. The internal effectiveness factor can then be expressed as:

$$\eta = \frac{1}{\phi}\cdot\frac{I1(2\phi\sqrt{e^{\gamma\alpha\delta}}/\gamma\alpha\delta)\cdot K1(2\phi/\gamma\alpha\delta) - K1(2\phi\sqrt{e^{\gamma\alpha\delta}}/\gamma\alpha\delta)\cdot I1(2\phi/\gamma\alpha\delta)}{I0(2\phi/\gamma\alpha\delta)\cdot K1(2\phi\sqrt{e^{\gamma\alpha\delta}}/\gamma\alpha\delta) + K0(2\phi/\gamma\alpha\delta)\cdot I1(2\phi\sqrt{e^{\gamma\alpha\delta}}/\gamma\alpha\delta)} \quad (13)$$

where the updated Thiele modulus was computed as the ratio between surface reaction rate and the diffusion rate:

$$\phi^2 = \frac{k_i\cdot\delta^2}{D_{eff}}\cdot\left(\frac{\alpha\Phi_0}{Bp_0n_0\hbar\omega}\right)^{\gamma} \quad (14)$$

The internal effectiveness factor is plotted for both models in Fig. 11. η_{LIM} accounts only for mass transfer limitation, while η_{LDM} considers both diffusion and radiative transport when assessing catalyst coverage. The relative effectiveness factor is an indication for which transport is limiting. While in the top layer light and consequently, reaction rate are controlling, when the relative effectiveness factor levels off, mass transfer takes over and no further improvement in conversion can be sought. It can be noticed that the thickness corresponding to the transition between the two regimes is the same for which conversion reached its maximum in Fig. 7. Hence, the relative effectiveness factor can be considered the absolute performance parameter for immobilized photocatalytic reactors.

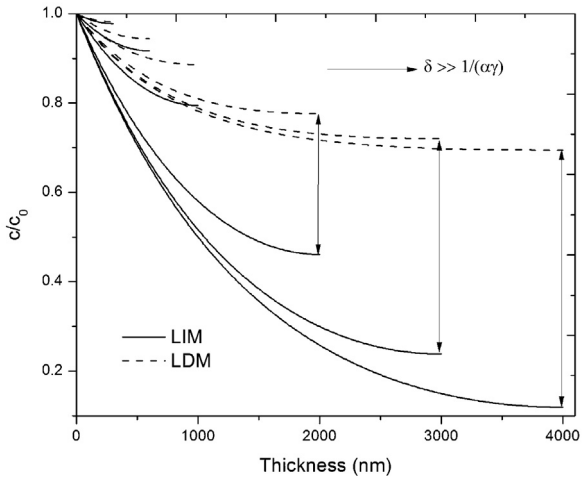

Fig. 10. Normalized concentration profiles vs. catalyst thickness. $k = 69.485\ s^{-1}$ for LIM, $k_i = 6.46\times10^{-48}\ s^{-1}$, $\alpha = 1.073\times10^{6}$ 1/m, $\gamma = 1$, $\Phi_0 = 180\ W/m^2$ for LDM.

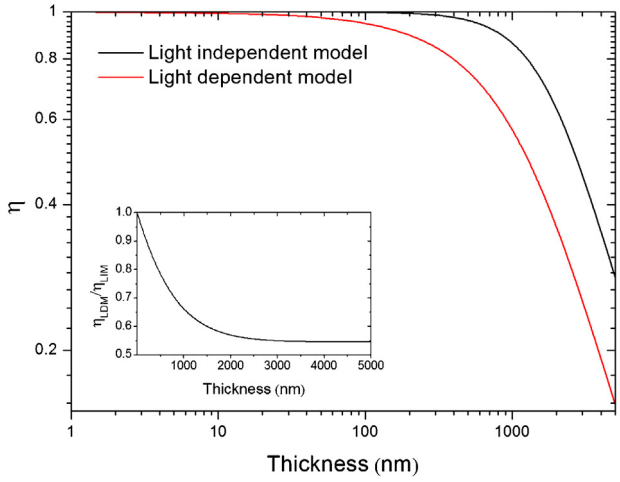

Fig. 11. Internal effectiveness factor vs. catalyst thickness. $k = 69.485\ s^{-1}$ for LIM, $k_i = 6.46\times10^{-48}\ s^{-1}$, $\alpha = 1.073\times10^{6}$ 1/m, $\gamma = 1$, $\Phi_0 = 180\ W/m^2$ for LDM. The insert shows the LDM/LIM effectiveness factor.

The maximum conversion thickness depends on the absorption coefficient and incoming photon flux density. For higher α, the initial decrease becomes steeper, lowering the maximum conversion thickness. For higher light intensities, the maximum conversion thickness is also decreasing due to the higher $k_{y=0}$. The difference is in the asymptotic value for the relative effectiveness factor which suggests how far away the two models are from each other. For higher α the discrepancy between the two models is increasing, while for higher light intensities it is decreasing.

5. Conclusions

Accurate modeling for microreactors can be achieved by applying basic physical mechanisms. This leads to a rational reactor design and easy optimization. The present article attempts a complete model for immobilized photocatalytic microreactors and explores their potential as investigation tools for intrinsic kinetics.

Models capable of describing reactor performance were build for a first order reaction rate with either light independency or light dependency described by photon absorption carrier generation mechanism. The extracted reaction rate constant reveals the intrinsic kinetics as both external and internal mass transport are accounted for. For the first time k values on the order of magnitude $10^1\ s^{-1}$ are reported.

The simplification to the light independent model is justified by defining a criterion for neglecting light intensity based on film thickness and absorption coefficient. Performance parameters are also derived for the situation when irradiance has to be considered. The updated internal effectiveness factor reveals both mass transfer and light limitations.

Acknowledgements

This work is supported by NanoNextNL, a micro and nanotechnology consortium of the Government of the Netherlands and 130 partners.

References

[1] T.V. Gerven, G. Mul, J. Moulijn, A. Stankiewicz, Chemical Engineering and Processing: Process Intensification 46 (2007) 781–789.
[2] S.B. Kim, S.C. Hong, Applied Catalysis B: Environmental 35 (2002) 305–315.
[3] K. Natarajan, T.S. Natarajan, H. Bajaj, R.J. Tayade, Chemical Engineering Journal 178 (2011) 40–49.
[4] H. Yang, G. Li, T. An, Y. Gao, J. Fu, Catalysis Today 153 (2010) 200–207.
[5] G. Plantard, F. Correia, V. Goetz, Journal of Photochemistry and Photobiology A: Chemistry 222 (2011) 111–116.
[6] F. Shahrezaei, Y. Mansouri, A.A.L. Zinatizadeh, A. Akhbari, Powder Technology 221 (2012) 203–212.
[7] G.S. Shephard, S. Stockenstram, D. de Villiers, W.J. Engelbrecht, G.F. Wessels, Water Research 36 (2002) 140–146.
[8] R. Wang, D. Ren, S. Xia, Y. Zhang, J. Zhao, Journal of Hazardous Materials 169 (2009) 926–932.
[9] W.-Y. Wang, A. Irawan, Y. Ku, Water Research 42 (2008) 4725–4732.
[10] Z. Zhang, H. Wu, Y. Yuan, Y. Fang, L. Jin, Chemical Engineering Journal 184 (2012) 9–15.
[11] S. Ahmed, M. Rasul, R. Brown, M. Hashib, Journal of Environmental Management 92 (2011) 311–330.
[12] M.N. Chong, B. Jin, C.W. Chow, C. Saint, Water Research 44 (2010) 2997–3027.
[13] M.L. Satuf, M.J. Pierrestegui, L. Rossini, R.J. Brandi, O.M. Alfano, Catalysis Today 161 (2011) 121–126.
[14] M.L. Satuf, R.J. Brandi, A.E. Cassano, O.M. Alfano, Catalysis Today 129 (2007) 110–117.
[15] C. Passalia, O.M. Alfano, R.J. Brandi, Journal of Hazardous Materials 212 (2012) 357–365.
[16] J. Marugan, R. van Grieken, C. Pablos, M.L. Satuf, A.E. Cassano, O.M. Alfano, Chemical Engineering Journal 224 (2013) 39–45.
[17] J. Marugan, R. van Grieken, A.E. Cassano, O.M. Alfano, Catalysis Today 144 (2009) 87–93.
[18] J. Marugan, R. van Grieken, A.E. Cassano, O.M. Alfano, Applied Catalysis B: Environmental 85 (2008) 48–60.
[19] N. Doucet, O. Zahraa, M. Bouchy, Catalysis Today 122 (2007) 168–177.
[20] J.E. Duran, M. Mohseni, F. Taghipour, Chemical Engineering Science 65 (2010) 1201–1211.
[21] M. Mohseni, F. Taghipour, Chemical Engineering Science 59 (2004) 1601–1609.
[22] J. Moreira, B. Serrano, A. Ortiz, H. de Lasa, Chemical Engineering Science 78 (2012) 186–203.
[23] M.A. Mueses, F. Machuca-Martinez, G.L. Puma, Chemical Engineering Journal 215–216 (2013) 937–947.
[24] R.L. Pozzo, R.J. Brandi, A.E. Cassano, M.A. Baltanais, Chemical Engineering Science 65 (2010) 1345–1353.
[25] M. de los Milagros Ballari, R. Brandi, O. Alfano, A. Cassano, Chemical Engineering Journal 136 (2008) 242–255.
[26] M. de los Milagros Ballari, R. Brandi, O. Alfano, A. Cassano, Chemical Engineering Journal 136 (2008) 50–65.
[27] M. de los Milagros Ballari, O.M. Alfano, A.E. Cassano, Chemical Engineering Science 65 (2010) 4931–4942.
[28] M. Motegh, J. Cen, P.W. Appel, J.R. van Ommen, M.T. Kreutzer, Chemical Engineering Journal 208 (2012) 607–615.
[29] C. Arancibia-Bulnes, S. Cuevas, Solar Energy 76 (2004) 615–622.
[30] R.J. Brandi, M.A. Citroni, O.M. Alfano, A.E. Cassano, Chemical Engineering Science 58 (2003) 979–985.
[31] G.E. Imoberdorf, F. Taghipour, M. Keshmiri, M. Mohseni, Chemical Engineering Science 63 (2008) 4228–4238.
[32] G.L. Puma, A. Brucato, Catalysis Today 122 (2007) 78–90.
[33] G. Li Puma, Environmental Science & Technology 37 (2003) 5783–5791.
[34] F. Jovic, V. Kosar, V. Tomasic, Z. Gomzi, Chemical Engineering Research and Design 90 (2012) 1297–1306.
[35] K. Demeestere, A.D. Visscher, J. Dewulf, M.V. Leeuwen, H.V. Langenhove, Applied Catalysis B: Environmental 54 (2004) 261–274.
[36] G.L. Puma, P.L. Yue, Chemical Engineering Science 58 (2003) 2269–2281.
[37] G.L. Puma, P.L. Yue, Chemical Engineering Science 56 (2001) 2733–2744.
[38] G.L. Puma, P.L. Yue, Chemical Engineering Science 53 (1998) 2993–3006.
[39] G.E. Imoberdorf, H.A. Irazoqui, O.M. Alfano, A.E. Cassano, Chemical Engineering Science 62 (2007) 793–804.
[40] G.E. Imoberdorf, A.E. Cassano, H.A. Irazoqui, O.M. Alfano, Catalysis Today 129 (2007) 118–126.
[41] V. Tomasic, F. Jovic, Z. Gomzi, Catalysis Today 137 (2008) 350–356.
[42] I. Salvado-Estivill, A. Brucato, G. Li Puma, Industrial & Engineering Chemistry Research 46 (2007) 7489–7496.
[43] Z. Wang, J. Liu, Y. Dai, W. Dong, S. Zhang, J. Chen, Journal of Hazardous Materials 216 (2012) 25–31.
[44] M. Dijkstra, H. Panneman, J. Winkelman, J. Kelly, A. Beenackers, Chemical Engineering Science 57 (2002) 4895–4907.
[45] K. Mehrotra, G.S. Yablonsky, A.K. Ray, Chemosphere 60 (2005) 1427–1436.
[46] A.A. Assadi, J. Palau, A. Bouzaza, D. Wolbert, Chemical Engineering Research and Design 91 (2013) 1307–1316.
[47] A.A. Assadi, A. Bouzaza, D. Wolbert, Journal of Photochemistry and Photobiology A: Chemistry 236 (2012) 61–69.
[48] B. Boulinguiez, A. Bouzaza, S. Merabet, D. Wolbert, Journal of Photochemistry and Photobiology A: Chemistry 200 (2008) 254–261.
[49] V. Goetz, J. Cambon, D. Sacco, G. Plantard, Chemical Engineering and Processing: Process Intensification 48 (2009) 532–537.
[50] R. Gorges, S. Meyer, G. Kreisel, Journal of Photochemistry and Photobiology A: Chemistry 167 (2004) 95–99.
[51] Y. Matsushita, N. Ohba, S. Kumada, K. Sakeda, T. Suzuki, T. Ichimura, Chemical Engineering Journal 135 (Suppl. 1) (2008) S303–S308.
[52] L. Lei, N. Wang, X.M. Zhang, Q. Tai, D.P. Tsai, H.L.W. Chan, Biomicrofluidics 4 (2010) 31–43.
[53] Z. Meng, X. Zhang, J. Qin, Nanoscale 5 (2013) 4687–4690.
[54] H. Lindstrom, R. Wootton, A. Iles, AIChE Journal 53 (2007) 695–702.
[55] G. Charles, T. Roques-Carmes, N. Becheikh, L. Falk, J.-M. Commenge, S. Corbel, Journal of Photochemistry and Photobiology A: Chemistry 223 (2011) 202–211.
[56] M.G. Nielsen, S.-I. In, P.C. Vesborg, T. Pedersen, K.P. Almtoft, I.H. Andersen, O. Hansen, I. Chorkendorff, Journal of Catalysis 289 (2012) 62–72.
[57] D.A.G. Bruggeman, Annalen der Physik 416 (1935) 636–664.
[58] B. Johs, J.S. Hale, Physica Status Solidi (a) 205 (2008) 715–719.
[59] J. Kasanen, J. Salstela, M. Suvanto, T.T. Pakkanen, Applied Surface Science 258 (2011) 1738–1743.
[60] B.I. Stefanov, N.V. Kaneva, G.L. Puma, C.D. Dushkin, Colloids and Surfaces A: Physicochemical and Engineering Aspects 382 (2011) 219–225.
[61] S. Zhang, Z. Chen, Y. Li, Q. Wang, L. Wan, Catalysis Communications 9 (2008) 1178–1183.
[62] H. Xu, M. Li, Z. Jun, Materials Research Bulletin 48 (2013) 3144–3148.
[63] Y. Wang, J. Lin, R. Zong, J. He, Y. Zhu, Journal of Molecular Catalysis A: Chemical 349 (2011) 13–19.
[64] L. Rizzo, J. Koch, V. Belgiorno, M. Anderson, Desalination 211 (2007) 1–9.
[65] H. Lachheb, E. Puzenat, A. Houas, M. Ksibi, E. Elaloui, C. Guillard, J.-M. Herrmann, Applied Catalysis B: Environmental 39 (2002) 75–90.
[66] A. Khataee, M. Fathinia, S. Joo, Spectrochimica Acta Part A: Molecular and Biomolecular Spectroscopy 112 (2013) 33–45.
[67] K.-J. Hwang, J.-W. Lee, W.-G. Shim, H.D. Jang, S.-I. Lee, S.-J. Yoo, Advanced Powder Technology 23 (2012) 414–418.
[68] J. Choi, H. Lee, Y. Choi, S. Kim, S. Lee, S. Lee, W. Choi, J. Lee, Applied Catalysis B: Environmental 147 (2014) 8–16.
[69] H. Aran, D. Salamon, T. Rijnaarts, G. Mul, M. Wessling, R. Lammertink, Journal of Photochemistry and Photobiology A: Chemistry 225 (2011) 36–41.
[70] J.-M. Herrmann, Applied Catalysis B: Environmental 99 (2010) 461–468.
[71] G. Camera-Roda, F. Santarelli, Catalysis Today 129 (2007) 161–168.